ISSN (Print) : 0974-6846
Indian Journal of Science and Technology, *Vol 9(11), DOI: 10.17485/ijst/2016/v9i11/89389, March 2016* ISSN (Online) : 0974-5645

Design of Coordinated Control Scheme for Hybrid Resonant Boost Converter and Multi Level Inverter

J. Prakash[1*], Sarat Kumar Sahoo[2] and K. R. Sugavanam[3]

[1]Department of Electrical and Electronics Engineering, R. M. K College of Engineering and Technology, Chennai - 601206, Tamil Nadu, India; prakash_ies@yahoo.co.in
[2]Department of Electrical and Electronics Engineering, School of Electrical Engineering VIT University, Vellore - 632014, Tamil Nadu, India; sarata1@rediffmail.com
[3]Department of Electrical and Electronics Engineering, Vel Tech High Tech Dr. Rangarajan Dr. Sakunthala Engineering College, Chennai - 600062, Tamil Nadu, India; sugavanamkr@gmail.com

Abstract

Background/Objectives: This paper focus on Coordinated Control Scheme (CCS) for solar photovoltaic system using Hybrid Resonant Boost (HRB) converter and multilevel inverter. **Methods/Statistical Analysis:** The Maximum power point tracking has been implemented using Modified Perturb and Observe (MPO) algorithm. MPO algorithm mitigates the output power oscillation and maintain the Photovoltaic panel at maximum operating point. **Findings:** The HRB converter feeds a DC power to Modified nine level inverter to maintain the quality sinusoidal output. It also reduces the level of harmonics in the output to maintain the system output within standard level. Zero Current Switching (ZCS), Zero Voltage Switching (ZVS) and HRB topologies has been simulated using MATLAB/SIMULINK. The simulation results are used to validate the function of CCS. **Applications:** The proposed system is implemented for off grid solar photovoltaic (PV) power plant model.

Keywords: Coordinated Control Scheme, Efficiency, HRB, MLI, PWM

1. Introduction

The output characteristic of a photovoltaic panel depends on certain conditions like temperature and illumination intensity. The output characteristic has a distinctive Maximum Power Point (MPP) at which the product of voltage-current is highest. To regulate the power flow to the Grid connected or Standalone Photovoltaic system should have a MPP tracking controller. The function of MPPT is to ensure highest efficiency level by operating of the system at the Maximum power point, irrespective of climatic changes. The Simulink model of a PV system with MPPT controller is investigated[1–4]. The MPPT controller consists of a buck or boost DC to DC converter to control the current and voltage[5–7]. This is made possible by proper form of duty-cycle to the control circuit. Conventional converters and algorithms are not vastly effective in terms of ripple content mitigation and controller response to track the MPP of a PV panel[8–12].

The interleaved boost converter topology is introduced to overcome the above said drawbacks, and to improve the overall conversion efficiency[13,14]. The reduction in switching losses by using interleaved buck converter is explained in this paper[15,16]. The design and implementation of interleaved boost converter using Sic diodes for PV application and fuel cell application are presented[17–19]. The effective reduction in overall switching losses of the converter, the resonant converter topology like Zero Current Switching (ZCS) and Zero Voltage Switching (ZVS) have been introduced and presented[20–22].

* *Author for correspondence*

The combination of ZCS and ZVS known as soft switching converter and combination of interleaved and soft switching known as hybrid interleaved boost converter are presented. The hybrid interleaved soft switching topology is to improve the overall performance of the converter such as conversion efficiency and speed of response. Generally, the solar photovoltaic system has separate controllers which are used for their control scheme in DC to DC converter and inverter. The control scheme for DC to DC converter is implemented using a dedicated digital controller[23]. Then the power conversion for inverter has also carried out using another digital controller[24,25]. The MLI topologies are investigated by the researchers due to its merits such as reduce in power rating and improved voltage levels[26–30]. This paper presents the coordinated control strategy by using a single digital controller for both HRB and MLI.

2. Design of Coordinated Control Strategy (CCS) for HRB and MLI

The block diagram of coordinated control strategy as shown in Figure 1. The proposed system considered two 230W PV panels for 1kW power generation. It's connected in series. The panel peak power is about 460W, which may vary with change in climate condition. The specification of TITANS6-60 is presented in Table 1. The PV panel output varies with respective to irradiation level and temperature. The various output levels of the TITANS6-60 PV panels are also shown in Table 1.

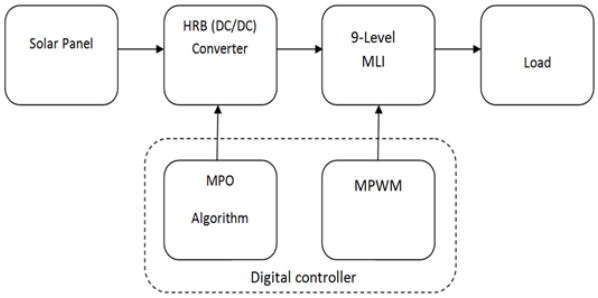

Figure 1. Generalized block diagram of the proposed CCS for solar PV system.

The proposed HRB converter with MPO algorithm is to improve the output of PV panel into the maximum level, by maintaining the MPP. This algorithm is used to identify the suitable duty cycle required by the converter to maintain the dc output voltage with very low ripple content. It also reduces the switching losses of the converter and improves the overall conversion ratio. The regulated DC output power from the HRB is fed to the modified multilevel inverter. Modified Pulse Width Modulation (PWM) scheme are implemented for this MLI. The simulation of CCS is carried out by using MATLAB/SIMULINK tools.

2.1 Design of Hybrid Resonant Boost Converter (HRB)

In general, the number of PV panels are required for standalone system to deliver the load power based on the load demand. For example, the 1 kW system requires a minimum of five panels of 230 W. In this case, the power will be met by two panels of same power rating by using HRB converter. The conventional converters have a conversion efficiency of 70% to 85% [10]. Hence they failed to achieve the desired output power or higher efficiency [10, 11, 12, 13, 14]. But the desired output can be achieved by the proposed HRB converter with negligible switching losses as shown in Figure 2 [18]. The design of passive circuit elements is made from the minimum and maximum output voltage variation from the panel (i.e., $V_{in}\,(min)$ = 50 V and $V_{in}\,(max)$ =74 V).

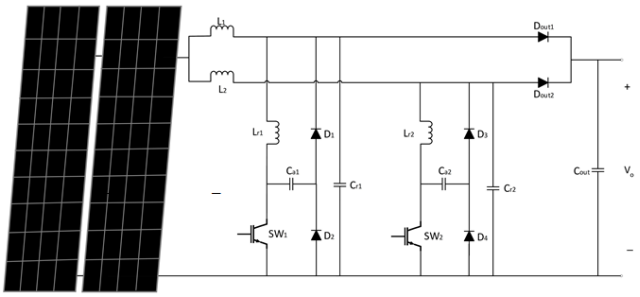

Figure 2. Hybrid resonant boost converter.

It is observed from the Figure 2 that, with the converter switching frequency as fsw=20 kHz, the variation of duty cycle is obtained as follows:

$$D = 1 - \left(\frac{V_0\ (panel)}{220} \right) \tag{1}$$

Thus, the range of the duty cycle to the HRB converter is found to be D(min) = 66.36% to D(max) = 77.27%. Based on these parameters, inductor and capacitors of HRB are calculated [26]. Table 1 shows the TITANS6-60 PV panel parameters.

Table 1. TITANS6-60 PV panel parameters at 25^{0}C, 1.5 AM, 1000 W/m2

Parameters	Values
I_{scn}	8.21 A
V_{ocn}	37.0 V
I_{mp}	7.44 A
V_{mp}	28.9 V
$P_{max,e}$	215.016 W
K_v	-0.123 V/K
K_i	3.18x10^{-3} A/K
N_s	60

2.2 Design of HRB Converter Circuit Elements

2.2.1 Inductor

By properly selecting the value of inductor of the boost converter, the output current ripple can be reduced to minimum level. This help in controlling the sudden changes in the input current as well as boosting the voltage and current during high switching frequencies.

$$L_1 = L_2 = \left(\frac{D \times V_{in} \times (1\text{-}D)}{2 \times f_{sw} \times I_{out}}\right) \quad (2)$$

The values of the resonant inductors are chosen based on the output and input voltage across the converter switch as follows.

$$L_{r1} = L_{r2} = \left(\frac{(V_{out} - V_{in} + V_d) \times (1\text{-}D)}{f_{sw} \times \text{min. } I_{out}}\right) \quad (3)$$

The eqn (4) determined the Peak value of inductor current.

$$I_{peak} = \left(\frac{V_{in\ max} \times D}{f_{sw} \times L}\right) \quad (4)$$

Using Eqns (2) to (4), the values of inductors are L1=L2=89.69 µH and Lr1=Lr2=56 µH.

where,

I_{out} = Output current from the converter in Amps

V_d = Diode voltage drop in Volts

$V_{in(max)=}$ Maximum input voltage to the converter in Volts

V_{out} = Output voltage from the converter in Volts

f_{sw} = Switching frequency of the converter in Hz

D = Duty cycle to the converter

2.2.2 Diode

The maximum output current which is equal to required forward current rating $I_f = I_{out}\,(max)$ i.e. 29.29A as the higher peak current rating is provided by Schottky diodes than average rating.

The power dissipation of the diode

$P_d = I_f * V_f$.

Where I_f is the boost converter diode forward current and V_f is forward voltage.

2.2.3 Capacitor

In a switching power supply, by keeping the input capacitor value at a minimum, the input voltage can be stabilized during the peak current requirement. Due to DC bias or temperature, Low Equivalent Series Resistance (ESR) ceramic capacitors are used to regulate the capacitance loss. To overcome the noise in the input voltage by increasing the value of capacitor with external compensation, the Eqn (5) is used to calculate the value of output capacitor for a desired output voltage with low ripple.

$$C_{out} > \left(\frac{I_{out}}{V_{ripple} \times f_{sw}}\right) \quad (5)$$

The Eqn (5) which is use to calculated the value of selected capacitance.

$$C_{r1} = \left(\frac{D_{min} \times (I_{max} - I_{min})}{\eth^2 \times L_r \times f_{sw}}\right) \quad (6)$$

The current rating of the capacitor is decided by the value of the resonant inductor. The Eqn (6) shows the value of resonant capacitor is selected based on the minimum and maximum current in the converter legs. The values of capacitors are calculated by using eqns (2 to4) and the values are C_{r1}=C_{r2}=10 µF and C_{out}=100 µF.

3. Modified Perturbation and Observation (P&O) Algorithm

The Perturbation and observation (P&O) method is efficient method as compared to traditional MPPT strategy. In P&O algorithm the step size has decided by the requirements of accuracy and tracking speed[10]. But

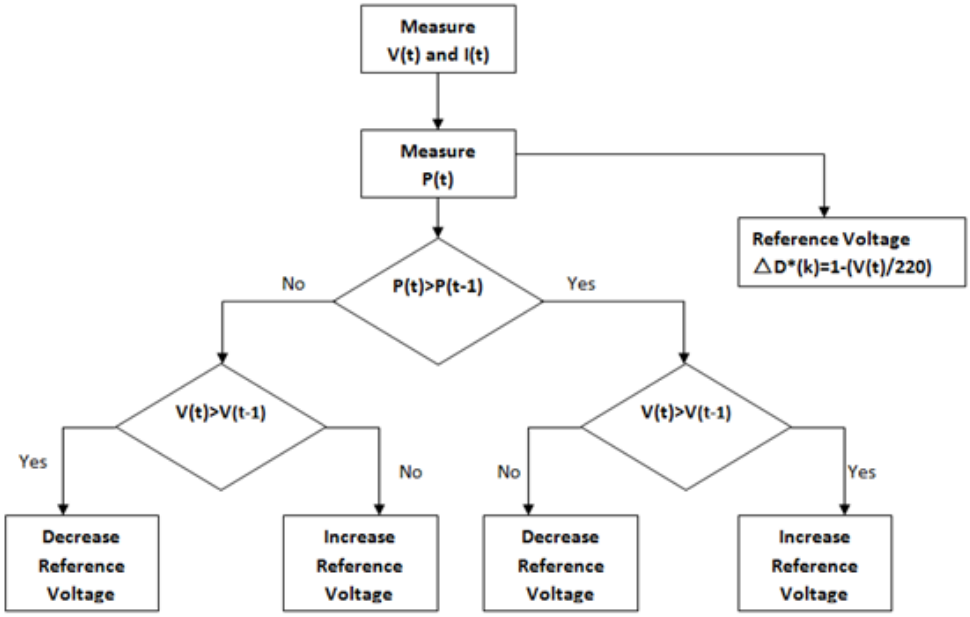

Figure 3. Functional flowchart of MPO algorithm.

P&O algorithm fail to track the maximum power during the fast varying atmospheric conditions[8–12]. To eliminate the drawbacks of conventional P&O algorithm. Modified P&O algorithm is proposed in this paper for the MPPT method. It is to overcome the shortcomings in usual MPPT algorithms as well as simple and highly effective way to improve the accuracy of tracking[6]. Modified P&O MPPT algorithm flow chart as shown in the Figure 3. According to operating point of a PV panel the firing angle of the converter is automatically varied[7,13,14].

Pseudo Code:

Functional unit name: MPO-MPPT
Input: Voltage and Current of a PV panel
Output: Duty cycle to the HRB
Steps:

1. Convert the given voltage and current into power and calculate the reference voltage.
2. If current power is greater than the previous power, then check current voltage greater than the previous voltage and then increase the increase the voltage reference of the output or vice versa.
3. Else if current power is less than the previous power, then check current voltage less than the previous voltage and then decrease the voltage reference of the output or vice versa.

End

Figure 4. Pseudo code for the MPO MPPT algorithm.

The switching frequency of the HRB converter is selected to be at 20 kHz. The initial duty cycle for the converter is fixed as 66.36% in order to reduce the output voltage ripples. To determine the MPP, the output power of the TITANS6-60 PV panel is calculated by sensing the voltage and current of the panel. Figure 4. shows the Pseudo code for the MPO implementation. Thus the converter duty cycle has been changed with respect to change in weather conditions like temperature and irradiation level.

4. Modified Multi Level Inverter Topology

The proposed circuit consists of a new nine level inverter topology for photovoltaic application. The conventional cascaded inverter topology needs 20 power switches and 24 switches in diode clamped arrangement for achieve 9 level output. But, the proposed MLI has required only seven IGBT switches in the power circuit. Figure 5. shows the dc link capacitor is used to divide the input voltage V_{dc} into four levels of each $V_{dc}/4$ magnitude. The proposed nine level Modified Multilevel inverter have four voltage divider capacitors such as C_1, C_2, C_3 & C_4 respectively (Figure 5). PWM signals were generated using pulsating DC Supply voltage and triangular carrier signal with various DC Offset are used to get four identical reference signals to generate PWM Signals. The operation of proposed MLI topology is explained and corresponding switching sequences are presented in Table 2. From the Table 2, it may be observed that the nine voltage levels can be generated from these voltage divider capacitors by controlling the seven IGBT switches with flow control diodes.

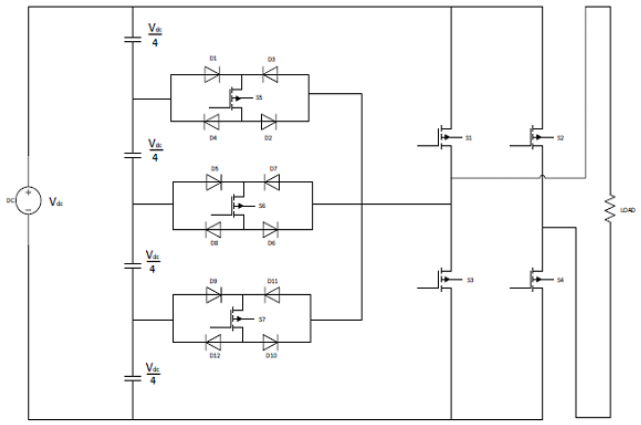

Figure 5. Schematic circuit of the 9-level Modified Multilevel inverter.

Table 2. Switching sequence for The Modified MLI

Mode	Switching Sequence	Voltage Level
I.	S_1 & S_4	$+V_{dc}$
II.	D_1, S_5, D_2 & S_4	$+3V_{dc}/4$
III.	D_5, S_6, D_6 & S_4	$+V_{dc}/2$
IV.	D_9, S_7, D_{10} & S_4	$+V_{dc}/4$
V	S_3 & S_4	$V_{dc}=0$
VI.	S_2, D_3, S_5& D_4	$-V_{dc}/4$
VII.	S_2, D_7, S_6 & D_8	$-V_{dc}/2$
VIII.	S_2, D_{11}, S_7 & D_{12}	$-3V_{dc}/4$
IX.	S_2 & S_3	$-V_{dc}$

The power switches are operated at nine different modes in order to achieve the 9-level. In mode 1, the MLI operated at maximum positive voltage i.e., V_{dc} by operating the switches $\boldsymbol{S_1}$=>$\boldsymbol{S_4}$. in mode 2, Voltage level has been reduced to the 3/4 by operating the switches in the following sequence $\boldsymbol{D_1}$=>$\boldsymbol{S_5}$=>$\boldsymbol{D_2}$=>$\boldsymbol{S_4}$. The schematic of the typical output voltage in 9-level inverter as shown in Figure 6 and Modified PWM switching patterns to the 9-Level inverter are shown in Figure 7.

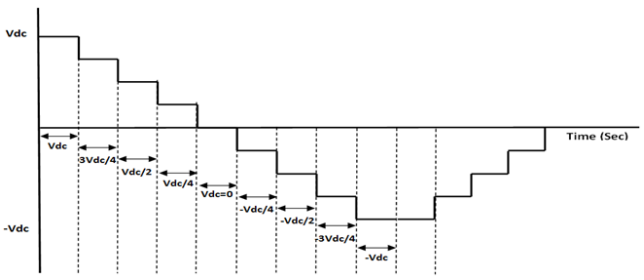

Figure 6. Schematic of the typical output voltage in 9-level inverter.

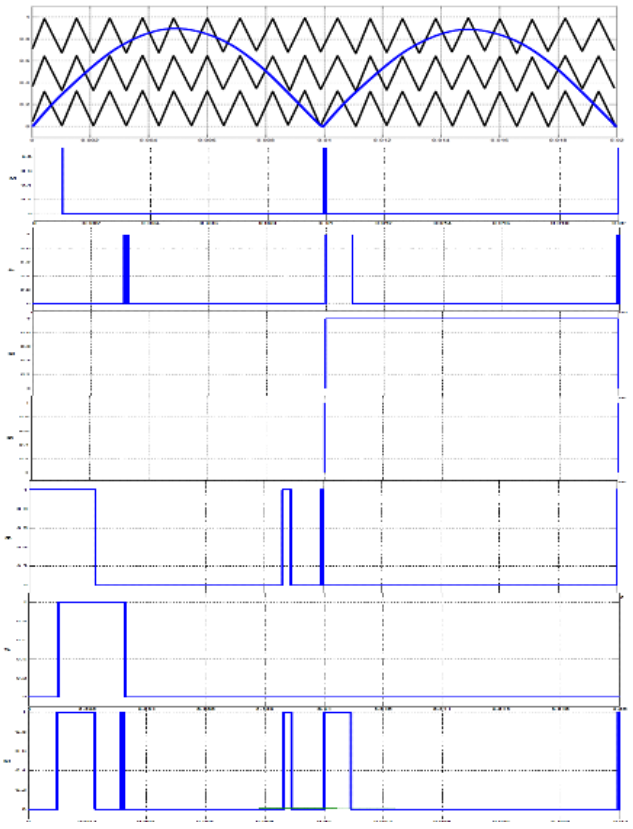

Figure 7. PWM switching patterns to the Modified 9-Level inverter.

The drawbacks in the conventional MLI topologies are overcome by the implementation of this modified 9-level inverter topology [24, 25]. The number of power switches can be reduced in proposed MLI with low power rating. Thus the switching losses and THD level at different operating frequencies (f_{sw}) has been reduced.

5. Implementation of Coordinated Control Strategy (CCS)

In this CCS, using single low cost digital controller the implementation of digital control of HRB and MLI can be achieved[31–34]. The separate digital controller is used to achieve the implementation of boost converter topology and also the implementation of MLI topologies are achieved using separate controller[35,36]. The main objective of the CCS is to attain the effective control operation by reducing the number of controllers used in the hardware and also the speed of the controller is taken

consideration for implementing this coordinated control logic. since the control logic for MPO-MPPT algorithm for HRB converter and the Modified PWM signals to the 9-Level inverter are runs in parallel for the entire control operation.

In PV system, the MPPT is a more sensitive process, since the output of PV panel is changed due to various factors like shadowing effect, irradiation and temperature. Even if the shadowing effect may be few micro seconds, during that time the output of the PV system becomes very low or zero. Thus the MPPT algorithm fails to track the MPP of the system during shadowing effect and generating oscillating output voltage in the DC to DC converter. It will affect the MLI output continuously. In this proposed system, the above said factors are considered during the selection of the control algorithm and controller. The MPO algorithm has an ability to meet out the above said requirement for the MPPT control and also the speed of operation to tracks the MPP within few micro seconds. According to the power variation from the panel the duty cycle to the converter can be changed. The control logic for the 9-Level inverter topology has been carried out using Modified PWM technique. The proposed CCS have operating speed of controller is about 5μS. Hence the oscillation of power from the panel is identified and overcome within short time.

6. Results and Discussion

The simulation for HRB and 9-level inverter for different operating conditions are carried out separately by using MATLAB/SIMULINK. Finally, the simulation of CCS for the HRB and 9-level inverter topology are carried out using MATLAB/SIMULINK environment. Using MPO MPPT algorithm the output of the HRB converter has been verified for the various climatic conditions. the output of the HRB is maximum level as compare with other resonant converter topologies like Zero voltage switching (ZVS) and Zero Current Switching (ZCS).

6.1 Simulation of HRB

The Figure 8 shows the Simulink model of the HRB converter and the comparative result of the, ZCS, ZVS and HRB as shown in Figure 11 to Figure 13.

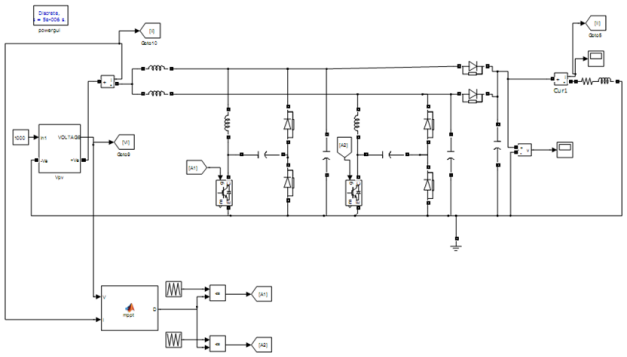

Figure 8. HRB converter Simulink model.

Modelling and simulation for proposed HRB converters are carried out using MATLAB Simulink environment. Here, the TITANS6-60 panel parameters as an input parameter for the PV panel model. This model will supply the power according to the climatic variation like irradiation level and temperature. Figure 9 and Figure 10 shows the variation of output from the PV panel is presented in I-V and P-V curves respectively. Further, Combined results of ZCS, ZVS and HRB output voltage waveforms at 25^0C and $250W/m^2$ is shown in Figure 11. Based upon the experimental data of TITANS6-60 panel as presented in Table 1, the design of converter elements and selection of duty cycle range are carried out and simulated using MATLAB/SIMULINK. The MPO algorithm helps the HRB converter efficiency is increased to 97.7% and mitigate the variation in output.

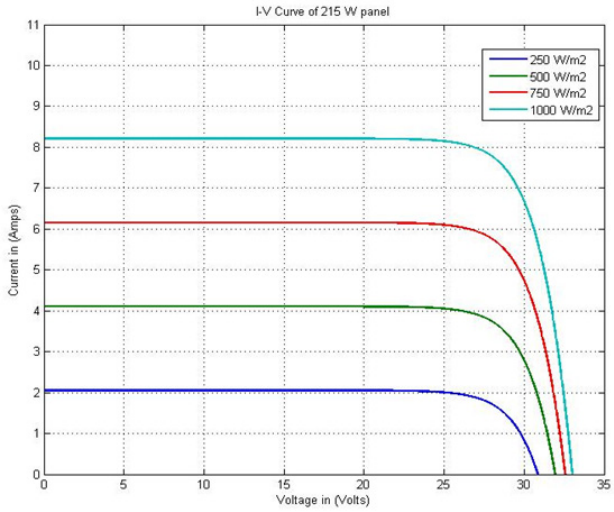

Figure 9. I-V Curves of TITANS6-60 panel at different Irradiation levels and 25^0C.

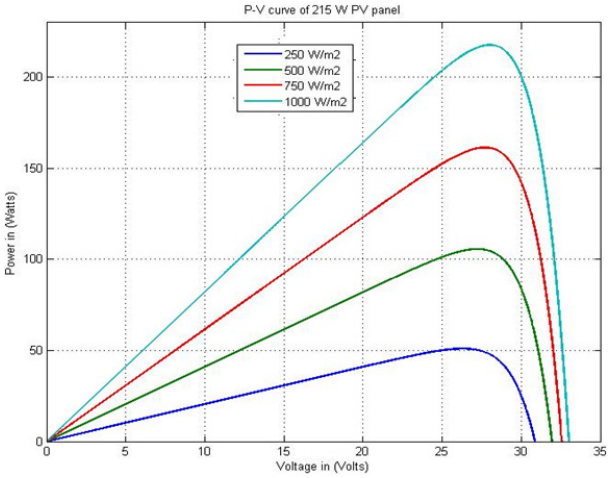

Figure 10. P-V curves of TITANS6-60 panel at different Irradiation levels and 25^{0}C.

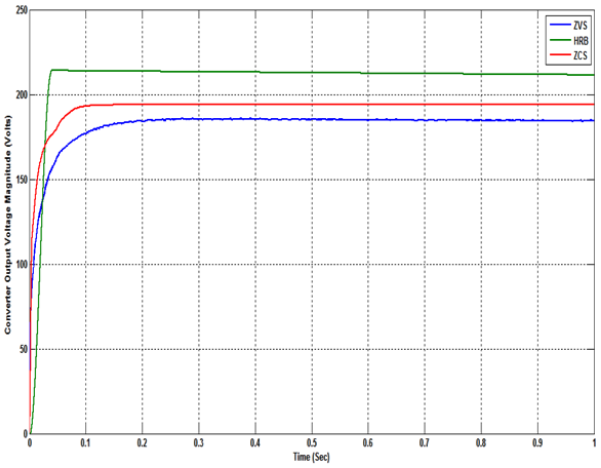

Figure 11. Combined results of ZCS, ZVS and HRB output voltage waveforms at 25^{0}C and 250W/m^2.

Figure 12 and Figure 13 shows the combined output voltage waveforms results of the ZCS, ZVS and HRB converter at different irradiation conditions. The results show, ZVS converter takes 0.25 sec to the settle the output without any damping for different irradiation level such as 250W/m^2, 500W/m^2 and 1000W/m^2 respectively. Similarly, the settling time of ZCS converter output is 0.1 sec without any damping by having the voltage magnitude of 190V at 250W/m^2, 210 V at 500W/m^2 and 220V at 1000W/m^2.

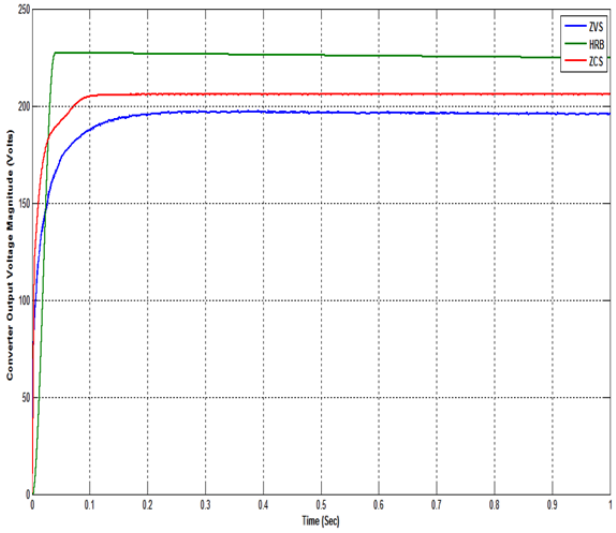

Figure 12. Combined results of ZCS, ZVS and HRB output voltage waveforms at 25^{0}C and 500W/m^2.

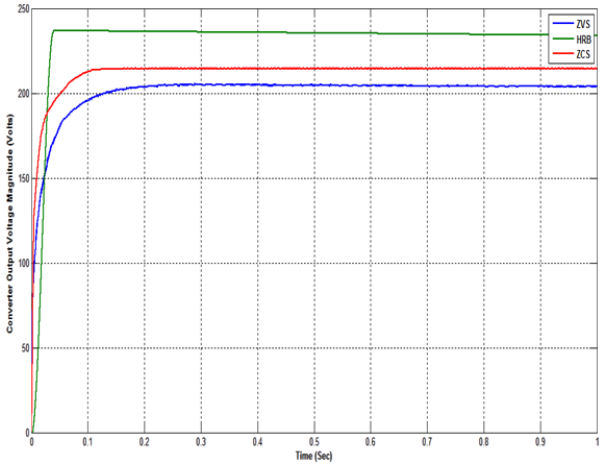

Figure 13. Combined results of ZVS, ZCS and HRB output voltage waveforms at 1000W/m^2 and 25^{0}C.

The proposed HRB converter have faster settling time and better conversion ratio as compared to ZVS and ZCS. Thus the HRB is achieved higher efficiency as well as reduces the switching losses. It is seen that the output DC voltage from the HRB is maintained nearly 230 V, which has a settling time of less than 20 ms at different input conditions.

6.2 Simulation of Modified 9-level Inverter Topology

The MATLAB Simulink model for the modified 9-level inverter topology is shown in Figure 14. The modified inverter circuit is analyzed at various operating frequencies. It was observed that, by using the digital PWM control, the magnitude of the output voltage steps is increased along with the reduction in the output harmonic level.

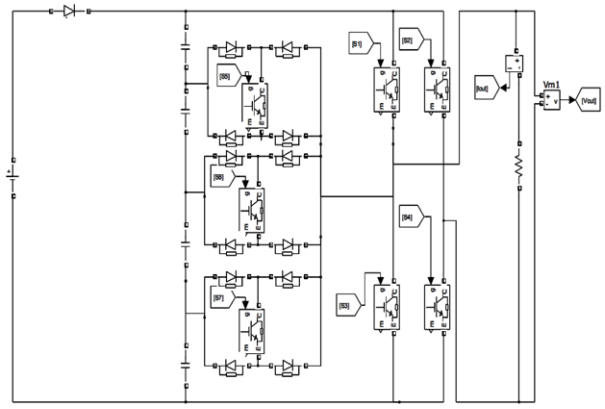

Figure 14. Simulink diagram of Modified 9-Level inverter.

The output waveform obtained from the 9-level inverter without filter is presented in Figure 15. HRB converter is the source of power to the MLI. The operating frequency (f_{sw}) of the HRB converter is maintained in a range of 1 kHz to 20 kHz, and hence the 9-level inverter has been analyzed for these operating frequencies to maintain the coordination between converter and inverter output voltage levels. This helps in the reduction of the THD in the inverter output and also the switching losses.

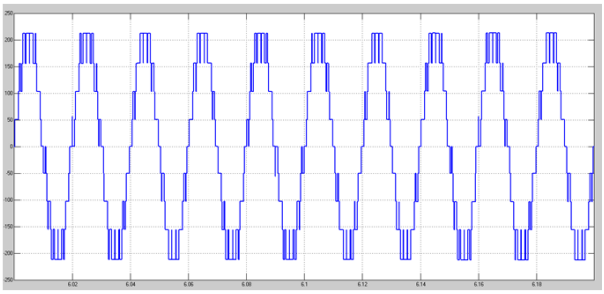

Figure 15. Output voltage waveform.

6.3 Simulation of CCS

The results shown in the Figures 16 to 20 depict a clear analysis of the performance of the CCS. Using MATLAB-SIMULINK circuit, the Coordinated control Scheme for the modified 9-level inverter and proposed HRB, is analysed. For analyzing the speed of the controller, the various parameter like irradiation and temperature changes in the HRB are varied along with the operating frequencies to the 9-level inverter.

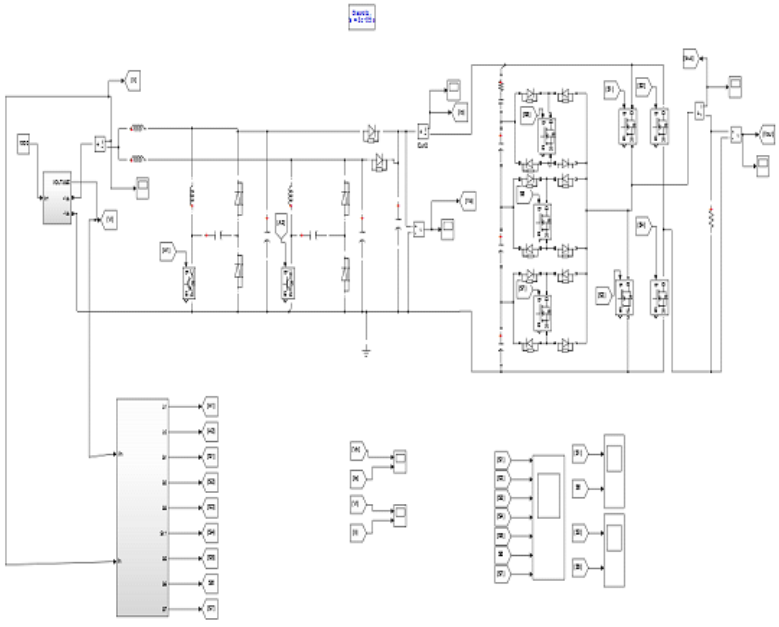

Figure 16. Matlab simulink model for coordinated control Scheme.

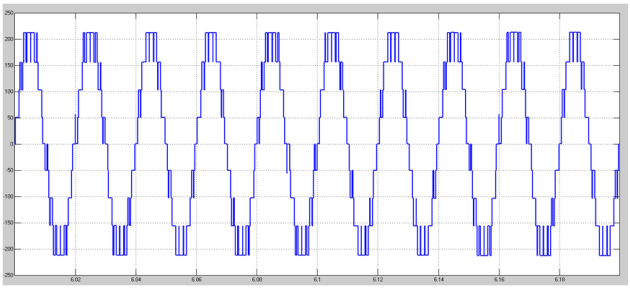

Figure 17. Output voltage waveform.

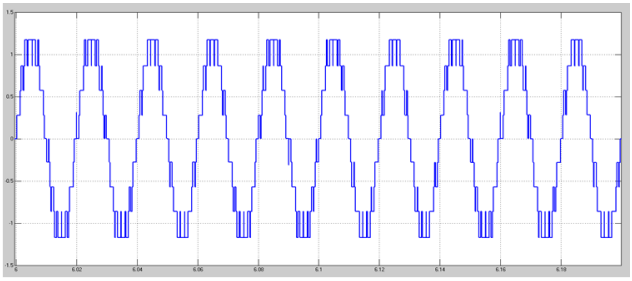

Figure 18. Output current waveform.

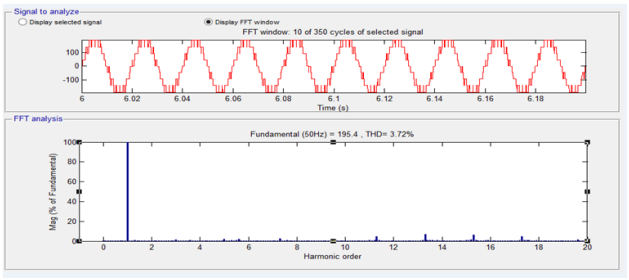

Figure 19. THD of output voltage.

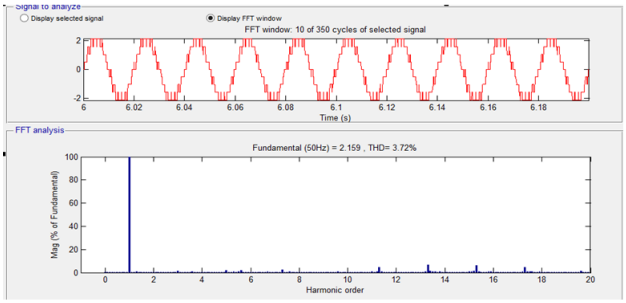

Figure 20. THD of output current.

Even with the fast varying input conditions like irradiation level and temperature, the performance of the HRB converter remains same. HRB is found to be taking 20ms to settle at the rated level which is shown in Figure 13. The THD level of CCS is 3.72% as shown in the Figure 20.

7. Conclusion

The circuit for the CCS for the HRB and 9-level inverter has been designed and implemented in MATLAB-SIMULINK. The circuits the operation of HRB, MLI and CCS are modeled and designed using MATLAB Software. The simulation is carried out by varying the input conditions such as various irradiation levels, temperatures and switching frequencies. The MPO algorithm is incorporated for MPPT control to HRB converter and Modified PWM control to the MLI. The effectiveness of the control is conformed through the simulation results. It is seen that the proposed CCS provides low THD, switching losses and improves overall efficiency of the converter which is found to be 97.9%. Thus we can conclude that the modified nine level inverter topology results in increasing the output voltage level along with reduced power rating of the switches. The added advantage is that this CCS can be implemented in a low cost digital controller.

8. References

1. Ahmed EM, Shoyama M. Variable step size maximum power point tracker using a single variable for stand-alone battery storage PV systems. Journal of Power Electronics. 2011; 11(2):218–27.
2. Sridhar R, Selvan JTN, Banerjee S. Modeling of PV array and performance enhancement by MPPT algorithm. International Journal of Computer Applications. 2010; 7(5):35–9.
3. El Shahat A. PV cell module modeling and ann simulation for smart grid applications. Journal of Theoretical and Applied Information Technology. 2010:9–20.
4. Hernanz RJA, Campayo Martín JJ, Belver IZ, Lesaka JL, Guerrero EZ, Pérez EP. Modeling of photovoltaic module. Proceedings of International Conference on Renewable Energies and Power Quality (ICREPQ'10); Granada: Spain; 2010. p. 1–5.
5. Jiang Y, Abu Qahouq JA, Batarseh I. Improved solar PV cell matlab simulation model and comparison. Proceedings of 2010 IEEE International Symposium on Circuits and Systems (ISCAS); Paris; 2010. p. 2770–3.
6. Mahdi AJ, Tang WH, Wu QH. Improvement of a MPPT algorithm for PV systems and its experimental validation. Proceeding International Conference on Renewable Energies and Power Quality (ICREPQ'10); Granada: Spain; 2010. p. 1–6.
7. Al-Diab A, Sourkounis C. Variable step size P&O MPPT algorithm for PV systems. Proceedings of 12th International Conference on Optimization of Electrical and Electronic Equipment, OPTIM; Basov; 2010. p. 1097–102.

8. Zainudin HN, Mekhilef S. Comparison study of maximum power point tracker techniques for PV systems. Proceedings of the 14th International Middle East Power Systems Conference (MEPCON'10); Cairo University: Egypt; 2010. p. 750–5.
9. Ren BY, Sun XD, Tong X, Zhong Y. Maximum power point tracking method based on the intermittent step-varied search for PV array. Proceedings of 2010 Asia-Pacific Power and Energy Engineering Conference (APPEEC); Chengdu; 2010. p. 1–4.
10. Petreus D, Moga D, Rusu A, Patarau T, Munteanu M. Photovoltaic system with smart tracking of the optimal working point. Advances in Electrical and Computer Engineering. 2010; 10(3):40–47.
11. Villalva MG, Gazoli JR, Filho ER. Comprehensive approach to modeling and simulation of photovoltaic arrays. IEEE Transactions on Power Electronics. 2009; 24(5):1198–208.
12. Tan CW, Green TC, Hernandez-Aramburo CA. Analysis of perturb and observe maximum power point tracking algorithm for photovoltaic applications. Proceedings of 2nd IEEE International Conference on Power and Energy (PECon' 08); Johor Bahru; 2008. p. 237–42.
13. Liu C, Wu B, Cheung R. Advanced algorithm for MPPT control of photovoltaic systems. Proceedings of Canadian Solar Buildings Conference; Montreal; 2004. p. 1–7.
14. Hohm DP, Ropp ME. Comparative study of maximum power point tracking algorithms. Progress in Photovoltaics: Research and Applications. 2003; 11(1):47–62.
15. Axelrod B, Berkovich Y, Ioinovici A. Switched-capacitor/switched-inductor structures for getting transformerless hybrid DCDC PWM converters. IEEE Transactions on Circuits and Systems I: Regular Papers. 2008; 55(2):687–96.
16. Lee IO, Cho S-Y, Moon G-W. Interleaved buck converter having low switching losses and improved step-down conversion ratio. IEEE Transactions on Power Electronics. 2012; 27(8):3664–75.
17. Ho CNM, Breuninger H, Pettersson S, Escobar G, Serpa LA, Coccia A. Practical design and implementation procedure of an interleaved boost converter using SiC diodes for PV applications. IEEE Transactions on Power Electronics. 2012; 27(6):2835–45.
18. Jung DY, Ji HH, Park S-H, Jung YC, Won CY. Interleaved soft-switching boost converter for photovoltaic power-generation system, IEEE Transactions on Power Electronics. 2011; 26(4):1137–45.
19. Samosir AS, Anwari M, Yatim AHM. Dynamic evolution control of interleaved boost dc-dc converter for fuel cell application. Proceedings of IPEC Conference 2010; Singapore; 2010. p. 869–74.
20. Lin BR, Chao CH, Chien CC. Interleaved boost-flyback converter with boundary conduction mode for power factor correction. Proceedings of 6th IEEE Conference on Industrial Electronics and Applications (ICIEA); Beijing; 2011. p. 1828–33.
21. Rezvanyvardom M, Adib E, Farzanehfard H. A new interleaved ZCS PWM boost converter. Proceedings of IEEE International Conference on Power and Energy, (PECon); Kulalumpur: Malaysia; 2010. p. 45–50.
22. Hsieh YC, Hsueh TC, Yen HC. An interleaved boost converter with zero-voltage transition. IEEE Transactions on Power Electronics. 2009; 24(4):973–78.
23. Pongiannan RK, Sathiyanathan M, Prakash A. FPGA realization of digital PWM controller using Q-format based signal processing. Journal of Vibration and Control. 2013.
24. Soto-Sanchez DE, Green TC. Voltage balance and control in a multi-level unified power flow controller. IEEE Transactions on Power Delivery. 2001; 16(4):732–38.
25. Pongiannan RK, Paramasivam S, Yadaiah N. Dynamically reconfigurable PWM controller for three phase voltage source inverters. IEEE Transactions on Power Electronics. 2010; 26(6):1790–9.
26. Make a simple boost converter [Internet]. [Cited 2015 Sep 25]. Available from: http://www.ladyada.net/library/diy-boostcalc.html.
27. Peng FZ. A generalized multilevel inverter topology with self voltage balancing. IEEE Transactions on Industry Applications. 2001; 37(2):611–18.
28. Kim ID, Nho EC, Kim HG, Ko JS. A generalized undeland snubber for flying capacitor multilevel inverter and converter. IEEE Transactions on Industrial Electronics. 2004; 51(6):1290–96.
29. Reddy M, Gowrimanohar T. Comparison of five level and seven level cascaded multilevel inverter based DSTACOM for compensation of harmonics and reactive power using instantaneous real-power theory. Proceedings of International Conference on Emerging Trends in Electrical Engineering and Energy Management (ICETEEEM); Chennai; 2012. p. 355–60.
30. Kabalci E, Colak I, Bayindir R, Pavlitov C. Modelling a 7-level asymmetrical h-bridge multilevel inverter with PS-SPWM control. Proceedings of International Aegan Conference on Electrical Machines and Power Electronics and Electromotion Joint Conference ACEMP. Istanbul – Turkey; 2011. p. 578–83.
31. Singh P, Tiwari S, Gupta KK. A new transistor clamped 5-level H-bridge multilevel inverter with voltage boosting capacity. Proceedings of 5th IEEE conference on Power India; 2012. p. 1–5.
32. Sadikin M, Senjyu T, Yona A. DC-DC type bidirectional high-frequency link DC for improved power quality of cascaded multilevel inverter. Proceedings of IEEE conference on Power and Energy (PECon); Kota Kinabalu Sabah: Malaysia; 2012. p. 49–54.
33. Dash PP, Kazerani M. Harmonic elimination in a multilevel current-source inverter-based grid-connected photovoltaic system. Proceedings of 38th Annual Conference on IEEE Industrial Electronics Society IECON 2012. Montreal: QC; 2012. p. 1001–6.
34. Karuppanan P, Mahapatra KK. FPGA based cascaded mul-

tilevel pulse width modulation for single phase inverter. Proceedings of 9th International Conference on Environment and Electrical Engineering (EEEIC); Prague: Czech Republic; 2010. p. 273–76.
35. Sarada S, Reddy LB, Balaji K. Real-time implementation of multi level inverter for 3P4W distribution network using ANFIS control. Indian Journal of Science and Technology. 2015 Nov; 8(30):1–6. doi: 10.17485/ijst/2015/v8i30/78761.
36. Mahalakshmi R, Thampatty KCS. Implementation of grid connected PV array using quadratic DC-DC converter and single phase multi level inverter. Indian Journal of Science and Technology. 2015 Dec; 8(35):1–7. doi: 10.17485/ijst/2015/v8i35/80548.